*R*esearch in
*A*stronomy and
*A*strophysics

The rate of period change in DAV stars

Yan-Hui Chen[1,2,3], Cai-Yun Ding[1,2,3], Wei-Wei Na[3,4] and Hong Shu[1,2,3]

[1] Institute of Astrophysics, Chuxiong Normal University, Chuxiong 675000, China; *yhc1987@cxtc.edu.cn*
[2] School of Physics and Electronical Science, Chuxiong Normal University, Chuxiong 675000, China
[3] Key Laboratory for the Structure and Evolution of Celestial Objects, Chinese Academy of Sciences, Kunming
    650011, China
[4] School of Physics and Electronic Engineering, Yuxi Normal University, Yuxi 653100, China

Abstract Grids of DAV star models are evolved by WDEC, taking the element diffusion effect into account. The grid parameters are hydrogen mass $\log(M_H/M_*)$, helium mass $\log(M_{He}/M_*)$, stellar mass M_* and effective temperature T_{eff} for DAV stars. The core compositions are from white dwarf models evolved by MESA. Therefore, DAV star models evolved by WDEC have historically viable core compositions. Based on those DAV star models, we studied the rate of period change ($\dot{P}(k)$) for different values of H, He, M_* and T_{eff}. The results are consistent with previous work. Two DAV stars G117–B15A and R548 have been observed for around 40 years. The rates of period change of two large-amplitude modes were obtained through the $O - C$ method. We conducted an asteroseismological study on the two DAV stars and then obtained a best-fitting model for each star. Based on the two best-fitting models, the mode identifications (l, k) of the observed modes for G117–B15A and R548 are consistent with previous work. Both the observed modes and the observed $\dot{P}$s can be fitted by calculated ones. The results indicate that our method of evolving DAV star models is feasible.

Key words: stars: oscillations (including pulsations) — stars: individual (G117-B15A and R548) — white dwarfs

1 INTRODUCTION

White dwarfs are the last observable stage of evolution for most low and medium mass stars. They comprise around 98% of the end state of all stars (Winget & Kepler 2008). Thermonuclear reactions have basically stopped inside a white dwarf. The central core temperature gradually decreases with the residual heat continually radiating from the surface. White dwarfs become darker and darker until we can no longer observe them. Field white dwarfs with a rich helium atmosphere are characterized as DO type (strong HeII lines) or DB type (strong HeI lines) white dwarfs, while those with a rich hydrogen atmosphere are characterized as DA type (only Balmer lines) white dwarfs (McCook & Sion 1999). Around 80% (Bischoff-Kim & Metcalfe 2011) of the population of field white dwarfs are DA type white dwarfs which have a layered structure due to element diffusion.

In the Hertzsprung-Russell diagram, there are DOV (around 170 000–75 000 K), DBV (around 29 000–22 000 K) and DAV (around 12 270–10 800 K) instability strips (Winget & Kepler 2008). At least 148 DAV stars have been observed (Castanheira et al. 2010). Details about the DAV instability strip are closely related to stellar gravitational acceleration (Gianninas et al. 2005, 2011). The instability strip is significantly wider for DAV stars with large gravitational accelerations. When DA type white dwarfs pass through the DAV instability strip, they will pulsate and change to DAV stars. These DAV stars cool down slowly and therefore the cooling rate is very small. Cooling and contraction produced by evolution can affect the pulsation periods. Therefore, it is very important to study the changing rate of pulsation periods, which can reflect the evolution of a star.

The cooling of a white dwarf is a very long process. The rate of period change is very small and not

easy to detect. Using Taylor's theorem in mathematics, astronomers have found a way to measure a minute rate of change, named $O - C$. The $O - C$ method means the observed minus calculated values, which treats the time of maximal light as a function of its cycle number. The $O - C$ method has been used to calculate the rate of period change in pre-white dwarf stars PG 0122+200 (Fu et al. 2002) and PG 1159–035 (Costa & Kepler 2008), DBV star EC 20058–5234 (Dalessio et al. 2013), and DAV stars G117–B15A (Kepler et al. 2000, 2005b; Kepler 2012) and R548 (Mukadam et al. 2013). The rate of period change can be used to measure the evolutionary rate of white dwarf stars (Kepler et al. 2005a).

Bradley & Winget (1991) discussed in detail the rate of period change in DBV and DAV stars with pure carbon cores. Studying the rate of period change in DAV stars with carbon/oxygen cores, Bradley et al. (1992) reported that the rates of period change for trapped modes were about half of the values for nontrapped modes. Bradley (1996) reported that the rate of period change was very sensitive to changes in the stellar mass and core compositions. An asteroseismological study including the rate of period change was conducted by Bradley (1998) for G117–B15A and R548, and by Bradley (2001) for L19-2 and GD165. Bischoff-Kim et al. (2008a) performed an asteroseismological study focusing on DAV stars G117–B15A and R548. They (Bischoff-Kim et al. 2008b) calculated the rate of period change for the best-fitting model of G117–B15A and tried to limit the axion mass. Giammichele et al. (2016) completed an asteroseismological study on R548 based on the optimization package genetic evolLUtion Code for asteroseismologY (LUCY). Based on new atmospheric modeling for DA white dwarfs, Giammichele et al. (2015) provided updated estimates of the time-averaged atmospheric properties of R548. The parameters of their best asteroseismological model are consistent with those of their best spectroscopical model, as shown in table 8 of Giammichele et al. (2016). The calculated rate of period change for the 213 s mode is consistent with the observed value obtained through $O - C$.

For model calculations, (k, l, m) are used to characterize an eigen-mode. The three indices are the radial order, the spherical harmonic degree and the azimuthal number, respectively. For DAV stars, the eigen-modes are non-radial g-mode pulsations. The rate of period change for pulsation periods with the same l value (usually $l = 1$ or 2) and the same m value ($m = 0$) can be calculated by

$$\dot{P}(k) = \frac{P_2(k) - P_1(k)}{\text{Age}_2 - \text{Age}_1}. \tag{1}$$

In Equation (1), $P_2(k)$ is the pulsation period of a DAV star with stellar age Age_2 and $P_1(k)$ is the pulsation period of the DAV star with stellar age Age_1. Precisely, $P_2(k)$ and $P_1(k)$ are the period of the same mode (same k) at two different epochs. $\dot{P}(k)$ can represent the corresponding rate of period (k) change.

MESA is a stellar evolution code reported by Paxton et al. (2011, 2013). A main-sequence (MS) star can be evolved into a white dwarf (WD) by MESA. The core compositions of a white dwarf result from thermal nuclear burning. However, DAV stars evolved by MESA usually have rich He/H envelopes. It is not convenient for MESA to evolve grids of DAV star models. WDEC is a quasi-static code to calculate the cooling process of white dwarf stars (Montgomery et al. 1999). Before the evolution, WDEC allows users to enter the hydrogen layer mass fraction ($\log(M_\text{H}/M_*)$), the helium layer mass fraction ($\log(M_\text{He}/M_*)$), the total stellar mass (M_*) and the effective temperature (T_eff) for the output white dwarfs. Namely, WDEC is suitable for evolving grids of white dwarf models. However, the core compositions are usually artificial, such as fully carbon (C), fully oxygen (O) or homogeneous C/O core compositions. Adding the core compositions of white dwarfs evolved by MESA into WDEC, grids of white dwarf models can be evolved by WDEC. Those white dwarf models have historically viable core composition profiles. The element diffusion scheme of Thoul et al. (1994) was included into WDEC by Su et al. (2014). This method has been used many times recently to evolve DAV stars (Chen & Li 2014b,a; Su et al. 2014; Chen 2016b) and DBV stars (Chen 2016a).

In this paper, we study the rate of period change in DAV stars based on the DAV star models evolved in the method. Based on observations spanning about 40 years, the rates of period change for two large-amplitude modes are obtained through the $O - C$ method (Kepler 2012; Mukadam et al. 2013). We try to check the DAV star models by conducting an asteroseismological study on the two DAV stars and comparing the calculated rates of period change to the observed values.

In Section 2, we briefly introduce the input physics and model calculations and discuss the $\dot{P}(k)$ values with various differences in stellar ages. We examine the rate of period change for DAV stars in Section 3, taking different values of H, He, M_* and T_eff into account. In Section 4, we conduct an asteroseismological study of DAV stars G117–B15A and R548, and then calculate the rates of period change for the two best-fitting models. The theoretical values of $\dot{P}(k)$ can be compared with the observed

values obtained through the $O − C$ method. Finally, we provide a discussion and conclusions in Section 5.

2 INPUT PHYSICS AND MODEL CALCULATIONS

We downloaded and installed the 6208 version of MESA. In the module 'make_co_wd', the initial MS stellar masses were entered, as shown in the first column of Table 1. The other input was the default values. The initial metal abundance was 0.02 and the mixing length parameter was 2.0. When the logarithm of stellar luminosity divided by solar luminosity was less than –2.0, those MS stars evolved to be WD stars. The corresponding WD masses are shown in the second column of Table 1. Those WDs usually have rich He/H envelopes. The core structure parameters, including mass, radius, luminosity, pressure, temperature, entropy and C profile, are extracted and added into WDEC. WDEC was first developed by Martin Schwarzschild and subsequently modified by Kutter & Savedoff (1969), Lamb & van Horn (1975) and Wood (1990). With opacities of Itoh et al. (1983, 1984), the equation of state is from Lamb (1974) and Saumon et al. (1995). In our calculations, standard mixing length theory is used and the mixing length parameter is adopted as $ML2/\alpha = 0.6$ for DAV stars. The core boundary of WDs evolved by MESA is defined around the peak of the C abundance. The O abundance equals one unit minus the C abundance. The corresponding core masses are shown in the third column of Table 1. With historically viable core compositions, grids of WDs can be evolved by WDEC. The composition profiles are results of diffusion, not the previous approximations of diffusion equilibrium H/He and He/C transitions (Su et al. 2014). The corresponding WD masses evolved by WDEC are shown in the fourth column of Table 1. The WD masses in the fourth column are around the values in the third column. It is an approximation in order to evolve more dense WD masses by WDEC. With a modified pulsation code of Li (1992b,a), full equations of linear and adiabatic oscillation are solved and the eigen-frequencies can be found one by one through scanning. Then, Equation (1) can be used to calculate the rate of period change.

In order to calculate $\dot{P}(k)$, two models with different ages should be selected. We choose typical DAV stars with $\log(M_H/M_*) = -4.0$, $\log(M_{He}/M_*) = -2.0$, $M_* = 0.600\,M_\odot$ and T_{eff} around 12 000 K. Four groups of DAV stars with different stellar ages are chosen, as shown in Figure 1. The abscissa is pulsation period $P(k)$ which is from 0 s to 1500 s. The ordinate is $\dot{P}(k)$.

Table 1 Masses of MS stars, WD stars, corresponding cores evolved by MESA and masses of corresponding WD stars evolved by WDEC.

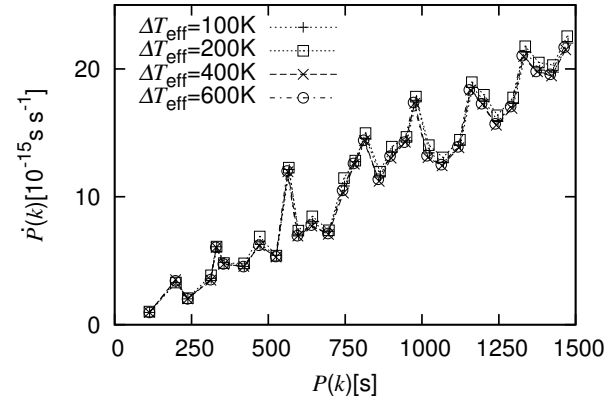| MS [$M_\odot$]	WD (MESA) [$M_\odot$]	M_{core}(MESA) [$M_\odot$]	WD (WDEC) [$M_\odot$]
3.00	0.579	0.550	0.550–0.560
3.20	0.599	0.575	0.565–0.585
3.40	0.627	0.600	0.590–0.610
3.50	0.652	0.625	0.615–0.635
3.60	0.675	0.650	0.640–0.660
3.70	0.694	0.675	0.665–0.685
3.80	0.714	0.770	0.690–0.710
3.92	0.738	0.725	0.715–0.735
4.00	0.763	0.750	0.740–0.750

Fig. 1 The rate of period change for models with different effective temperatures. The rate of period change is calculated by the difference of two eigen-periods (same k values) divided by the difference of corresponding model ages. The parameters of the models are $\log(M_H/M_*) = -4.0$, $\log(M_{He}/M_*) = -2.0$, $M_* = 0.600\,M_\odot$ and T_{eff} around 12 000 K. For example, the effective temperature is 12 050 K and 11 950 K for pluses and then ΔT_{eff} is 100 K.

The pluses, boxes, crosses and circles respectively correspond to DAV star models of $T_{eff} = 12 050\,K$ and 11 950 K, 12 100 K and 11 900 K, 12 200 K and 11 800 K, and 12 300 K and 11 700 K, respectively. Then, the values of $\dot{P}(k)$ can be calculated according to Equation (1). The radial order k is from 1 to 31 in the period range for those models.

In Figure 1, we can see that the values of $\dot{P}(k)$ are basically equal for $\Delta T_{eff} = 100$, 200, 400 and 600 K. We choose models of $\Delta T_{eff} = 400\,K$ to calculate the theoretical values of $\dot{P}(k)$ in this paper.

Some groups of DAV star models are evolved in order to study the rate of period change in DAV stars. For example, in order to study the effect of different values of H, we evolve DAV star models of $\log(M_H/M_*)$ from –10.0 to –4.0 with steps of 1.0, $\log(M_{He}/M_*) = -2.0$,

$M_* = 0.600\,M_\odot$, and $T_{\rm eff} = 12\,200\,{\rm K}$ and $11\,800\,{\rm K}$. In order to do the asteroseismological study on DAV star G117–B15A and R548, grids of DAV star models are evolved. The grid parameters are $\log(M_{\rm H}/M_*)$ from –10.0 to –4.0 with steps of 1.0, $\log(M_{\rm He}/M_*)$ from –4.0 to –2.0 with steps of 0.5, M_* from $0.550\,M_\odot$ to $0.750\,M_\odot$ with steps of $0.010\,M_\odot$, and $T_{\rm eff}$ from $12\,800\,{\rm K}$ to $10\,800\,{\rm K}$ with steps of $100\,{\rm K}$. After pre-selecting a pre-best-fitting model, the grids of DAV star models will be made dense around the pre-best-fitting parameters. Then, a best-fitting model will be selected. Finally, the calculated $\dot{P}(k)$ of the best-fitting model can be compared with the corresponding observed $\dot{P}$ through the $O-C$ method.

3 THE RATE OF PERIOD CHANGE IN DAV STARS

With the evolved DAV star models, we studied the rate of period change in DAV stars. Equation (1) is used on two DAV star models with differences in $T_{\rm eff}$ of 400 K. The pulsation code starts to calculate eigen-modes from $k = 1$. The lower k g-modes of each model will be calculated. We studied the effect of different values of H, He, kinetic energy distribution (KED), M_* and $T_{\rm eff}$ on the rate of period change. This may be helpful for qualitative analysis of the rate of period change in some observed stars.

3.1 The Effect of Different Values of H Atmosphere Mass and He Layer Mass

First of all, we studied the effect of different values of H atmosphere mass and He layer mass on the rate of period change in DAV stars.

In Figure 2, we show a diagram of $\dot{P}(k)$ versus $P(k)$ with different values of H atmosphere mass. With $T_{\rm eff} = 12\,200\,{\rm K}$ and $11\,800\,{\rm K}$, $\log(M_{\rm He}/M_*)$ is fixed to be -2.0, M_* is fixed to be $0.600\,M_\odot$ and $\log(M_{\rm H}/M_*)$ is from -10.0 to -4.0 with steps of 1.0. In the period range from 0 s to 1500 s, the radial order k is from 1 to 31 for the model of $\log(M_{\rm H}/M_*) = -4.0$ and from 1 to 23 for the model of $\log(M_{\rm H}/M_*) = -10.0$. The pulsation period is from 113.16 s ($k = 1$) to 1467.93 s ($k = 31$) for the model of $\log(M_{\rm H}/M_*) = -4$ and $T_{\rm eff} = 12\,200\,{\rm K}$. For models of $\log(M_{\rm H}/M_*) = -4$, and $T_{\rm eff} = 12\,200\,{\rm K}$ and $11\,800\,{\rm K}$, the differences in corresponding pulsation periods are from 0.92 s to 20.53 s and the difference of ages is 0.30×10^8 years. The rate of period change is from 0.97 to 21.70 in the unit of $10^{-15}\,{\rm s\,s^{-1}}$, marked as boxes in Figure 2.

The values of $\dot{P}(k)$ are all positive. This is because the cooling process dominates for cool white dwarfs, which will increase the degree of degeneracy and increase the pulsation period (Winget et al. 1983; Kepler et al. 2000; Winget & Kepler 2008). Overall, the rates of period change for different H atmosphere mass models basically overlap each other. We notice that the rate of period change is distributed in a strip from the lower left corner to the upper right corner. Basically, the longer the pulsation period is, the larger the rate of change for a period of a mode is. This is because the asymptotic period spacing is increasing with the white dwarf cooling down. The asymptotic period spacing (Tassoul 1980) can be calculated by

$$\Delta\bar{P}(l) = \frac{2\pi^2}{\sqrt{l(l+1)}\int_0^R \frac{|N|}{r}dr}. \qquad (2)$$

In Equation (2), R is stellar radius and N is Brunt-Väisälä frequency. Therefore, we basically have equations of

$$P(k) = P(k_0) + (k - k_0) \times \Delta\bar{P},$$
$$\text{and} \quad \dot{P}(k) = \dot{P}(k_0) + (k - k_0) \times \Delta\dot{\bar{P}}. \qquad (3)$$

We assume k_0 is so high that the value of $P(k_0)$ satisfies the asymptotic period spacing law. Therefore, periods with high k values will increase with both the cooling process of a DAV star and the increasing process of the asymptotic period spacing. The long-period modes should have a relatively large rate of period change.

In addition, some values of $\dot{P}(k)$ are located around the strip. For example, values represented by inverted triangles are relatively large around 1000 s and relatively small around 1250 s. This effect is associated with the mode trapping effect, which will be discussed in the next subsection.

These results are consistent with those of Bradley & Winget (1991). They found that the rate of period change for the model of $\log(M_{\rm H}/M_*) = -4.0$ was about half of that for the model of $\log(M_{\rm H}/M_*) = -10.0$. The conclusion is based on the abscissa being radial order k. However, the abscissa in Figure 2 is the pulsation period.

In Figure 3, we show the rate of period change for the radial order k. We can see that the values of $\dot{P}(k)$ for the model of $\log(M_{\rm H}/M_*) = -4.0$ are obviously smaller than those for the model of $\log(M_{\rm H}/M_*) = -10.0$. The frequency of an eigen-mode can be obtained from observations but the radial order k cannot be obtained. Therefore, diagrams of $\dot{P}(k)$ versus $P(k)$ are displayed in Figure 2.
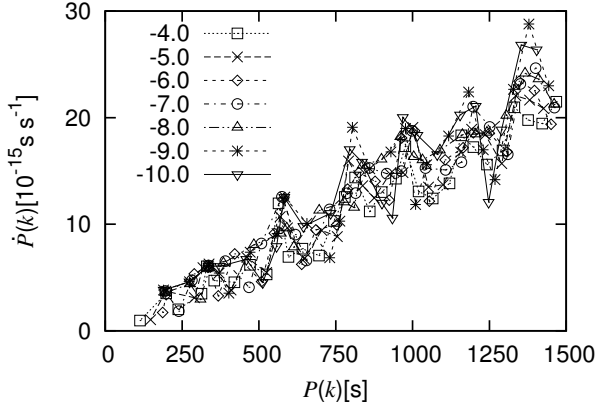
Fig. 2 The effect of different H atmosphere masses on the rate of period change. The parameters of the models are $\log(M_H/M_*)$ from -10.0 to -4.0 with steps of 1.0, $\log(M_{He}/M_*) = -2.0$, $M_* = 0.600\,M_\odot$, and $T_{eff} = 12\,200\,K$ and $11\,800\,K$.
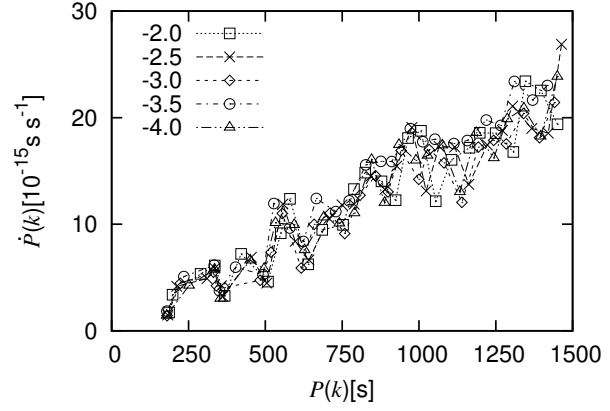

Fig. 4 The effect of different He layer masses on the rate of period change. The parameters of the models are $\log(M_H/M_*) = -6.0$, $\log(M_{He}/M_*)$ from -4.0 to -2.0 with steps of 0.5, $M_* = 0.600\,M_\odot$, and $T_{eff} = 12\,200\,K$ and $11\,800\,K$.
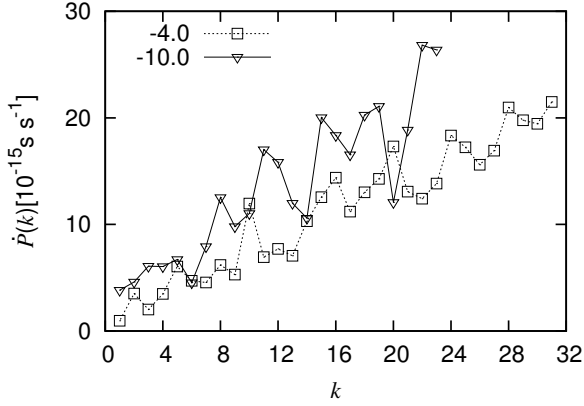

Fig. 3 The effect of different H atmosphere masses on the rate of period change. The abscissa is the radial order k. The squares and triangles are values for $\log(M_H/M_*)$.

In Figure 4, we show a diagram of $\dot{P}(k)$ versus $P(k)$ with different values of He layer mass. For the models, $\log(M_H/M_*)$ is -6.0, $\log(M_{He}/M_*)$ is from -4.0 to -2.0 with steps of 0.5, M_* is fixed to be $0.600\,M_\odot$, and T_{eff} equals $12\,200\,K$ and $11\,800\,K$. The radial order k is from 1 to 27 for the model of $\log(M_{He}/M_*) = -2.0$ and from 1 to 25 for the model of $\log(M_{He}/M_*) = -4.0$. The values of $\dot{P}(k)$ are not sensitive to different He layer masses, which are consistent with the results of Bradley & Winget (1991). They are distributed in a strip from the lower left corner to the upper right corner in Figure 4. There is also dispersion in some $\dot{P}(k)$ values around the strip.

3.2 The Effect of Kinetic Energy Distribution

Both different H models and different He models are found to have $\dot{P}(k)$s located around a strip. In this subsection, we try to discuss the rate of period change for each mode by analyzing its KED.

In Figure 5, we show the core composition profiles and the Brunt-Väisälä frequency of a DAV star model. The model parameters are $\log(M_H/M_*) = -4.0$, $\log(M_{He}/M_*) = -2.0$, $M_* = 0.600\,M_\odot$ and $T_{eff} = 11\,800\,K$. The C profile is from a $0.627\,M_\odot$ white dwarf ($0.600\,M_\odot$ core) evolved by MESA from a $3.40\,M_\odot$ MS star, as shown in Table 1. The white dwarfs evolved by MESA usually have rich He/H envelopes.

In the core, the O profile equals 1 minus the C profile. The H/He composition gradient zone and He/C/O composition gradient zone result from element diffusion. The composition transition zone can make a spike in the Brunt-Väisälä frequency. The spikes in the upper panel in Figure 5 lead to a mode trapping effect (Winget et al. 1981; Brassard et al. 1992). In addition, there is a thin convection zone on the surface in the upper panel.

In Figure 6, we show the rate of period change and corresponding KEDs of each mode. The model parameters are the same as in Figure 5. In order to calculate the rate of period change, models of $T_{eff} = 11\,800\,K$ and $12\,200\,K$ are evolved. The pulsation periods and corresponding KEDs are calculated for the model of $T_{eff} = 11\,800\,K$. The radial order k is from 1 to 31. The KEDs
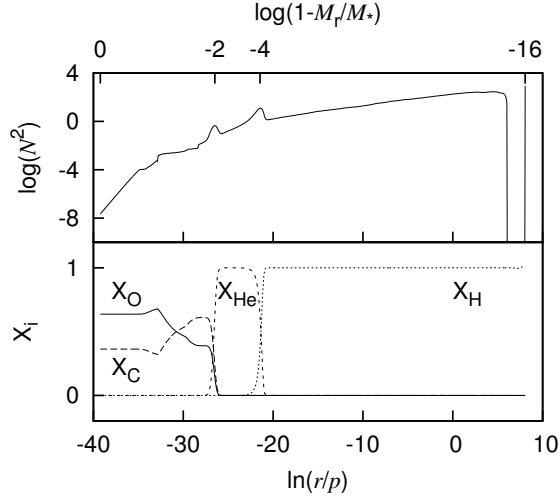
Fig. 5 The core composition profiles and the Brunt-Väisälä frequency for the model of $\log(M_{\mathrm{H}}/M_*) = -4.0$, $\log(M_{\mathrm{He}}/M_*) = -2.0$, $M_* = 0.600\,M_\odot$ and $T_{\mathrm{eff}} = 11\,800$ K.

Fig. 6 Diagram of the rate of period change vs. pulsation periods and corresponding KEDs. The model in the upper panel is the same as in Fig. 5. The value k is from 1 to 31. In the lower panel, two models of $T_{\mathrm{eff}} = 12\,200$ K and $11\,800$ K are used to calculate values of $\dot{P}(k)$.

can be calculated by,

$$
\begin{aligned}
&\mathrm{KED(C/O)/KED(He)/KED(H)}\\
=&4\pi \int_0^{R_{\mathrm{He/C/O}}} [(|\xi_r|^2 + l(l+1)|\xi_h|^2)]\rho_0 r^2 dr\\
&/4\pi \int_{R_{\mathrm{He/C/O}}}^{R_{\mathrm{H/He}}} [(|\xi_r|^2 + l(l+1)|\xi_h|^2)]\rho_0 r^2 dr\\
&/4\pi \int_{R_{\mathrm{H/He}}}^{R} [(|\xi_r|^2 + l(l+1)|\xi_h|^2)]\rho_0 r^2 dr.
\end{aligned}
\tag{4}
$$

In Equation (4), ρ_0 is the local density. KED(C/O), KED(He) and KED(H) respectively represent the value of kinetic energy for a given mode distributed in the C/O core, He layer and H atmosphere. $R_{\mathrm{He/C/O}}$, $R_{\mathrm{H/He}}$ and R are the locations of He/C/O interface, H/He interface and stellar radius, respectively.

For the model in Figures 5 and 6, $R_{\mathrm{He/C/O}}$ is the location of $\log(1 - M_{\mathrm{r}}/M_*) = -2.0$ and $R_{H/He}$ is the location of $\log(1 - M_{\mathrm{r}}/M_*) = -4.0$. As shown, for instance, in Christensen-Dalsgaard (2008), $\xi_r(r)$ is the radial displacement and $\xi_h(r)$ is the horizontal displacement. In the upper panel in Figure 6, total kinetic energy is set to be 1. KED(C/O) is represented by open dots and KED(H) is represented by crosses. Therefore, KED(He) equals 1 minus KED(C/O) and KED(H).

The radial order k is from 1 to 31 for the model, which can be inspected separately in Figure 6. For the modes with $k = 1, 3, 7, 9$ and 13, KED(H) is obviously larger than 50%. It means that those modes are trapped or partly trapped in the H atmosphere. They have minimal rates of period change in the lower panel. For the model
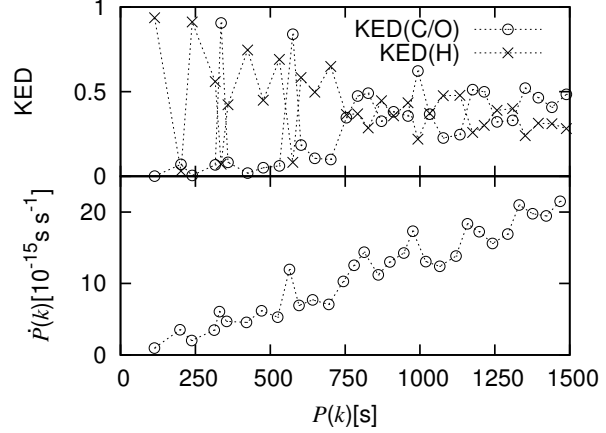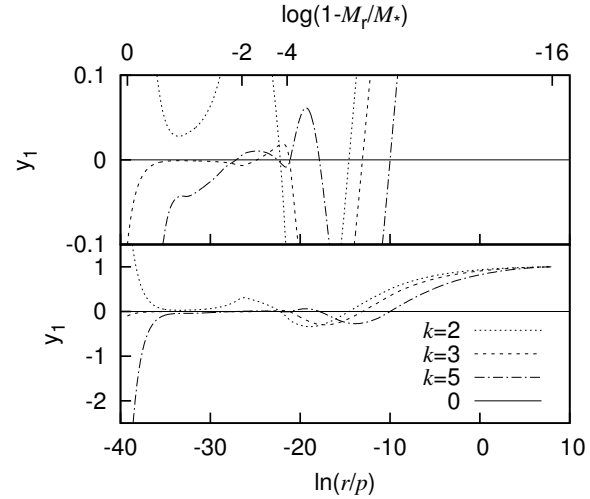

Fig. 7 Diagram of y_1 versus $\ln(r/p)$ for the modes of $k = 2, 3$ and 5. The model parameters are the same as in Fig. 5. The upper panel is a longitudinal enlargement of the lower one. The top abscissa is $\log(1 - M_{\mathrm{r}}/M_*)$, which shows the regions of C/O core, He layer and H atmosphere clearly.

of $k = 2$, both KED(C/O) and KED(H) are very small. Therefore, KED(He) is relatively large which means that the mode is trapped or partly trapped in the He layer. In the lower panel, $\dot{P}(k = 2)$ is maximal. For the modes of $k = 5, 10$ and 20, KED(C/O) is obviously larger than 50%. They are trapped or partly trapped in the C/O core and correspond to the maximal rates of period change in the lower panel. Namely, modes trapped or partly trapped in the C/O core or He layer have maximal $\dot{P}(k)$s. Modes trapped or partly trapped in the H atmosphere have min-
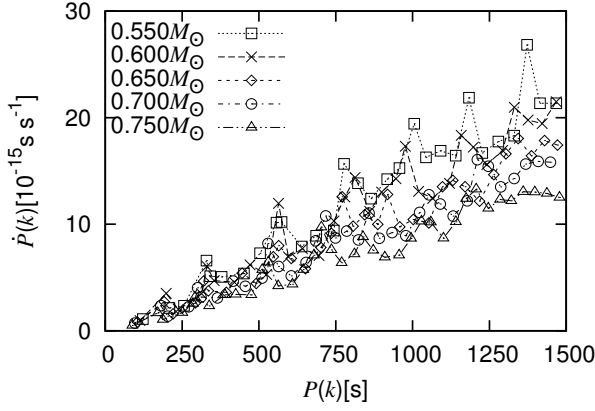
Fig. 8 The effect of different stellar masses on the rate of period change. The parameters of the models are $\log(M_\mathrm{H}/M_*) = -4.0$, $\log(M_\mathrm{He}/M_*) = -2.0$, M_* from $0.550\,M_\odot$ to $0.750\,M_\odot$ with steps of $0.050\,M_\odot$, and $T_\mathrm{eff} = 12\,200$ K and $11\,800$ K.

Fig. 9 The effect of different effective temperatures on the rate of period change. The parameters of the models are $\log(M_\mathrm{H}/M_*) = -4.0$, $\log(M_\mathrm{He}/M_*) = -2.0$, $M_* = 0.600\,M_\odot$ and T_eff from $12\,500$ K (± 200 K) to $10\,500$ K (± 200 K) with steps of 500 K.

imal $\dot{P}(k)$s. This is reasonable, because the cooling rate of the C/O core and He layer is faster than that of the H atmosphere; the cooling process dominates for DAV stars (Winget et al. 1983). Bradley et al. (1992) reported that the rates of period change for trapped modes (modes trapped or partly trapped in the H atmosphere) are about half the values for nontrapped modes. Different values of H atmosphere mass and He layer mass will affect the rate of period change by the mode trapping effect.

In Figure 7, we show a diagram of a variable y_1 versus the stellar structure parameter $\ln(r/p)$. In the abscissa, r is stellar local radius and p is stellar local pressure. The variable y_1 is a dimensionless variable of the radial displacement ξ_r,

$$y_1 = \frac{GM}{R^3}\frac{\xi_r}{g_r}. \tag{5}$$

In Equation (5), G is the gravitational constant, M is stellar mass and g_r is stellar local gravitation. The modes of $k = 2, 3$ and 5 are shown in the lower panel in Figure 7. The upper panel is an enlargement of the lower one. The values of k can be identified from the intersection points between y_1 and zero lines. The abscissa on the upper boundary is $\log(1 - M_\mathrm{r}/M_*)$. The modes of $k = 2, 3$ and 5 have their largest y_1 amplitude in the He layer, H atmosphere and C/O core, respectively. The top abscissa in Figure 7 shows the regions clearly.

3.3 The Effect of Different Values of Total Stellar Mass and Effective Temperature

From the above discussion, we understand that the mode trapping effect will affect the rate of period change up
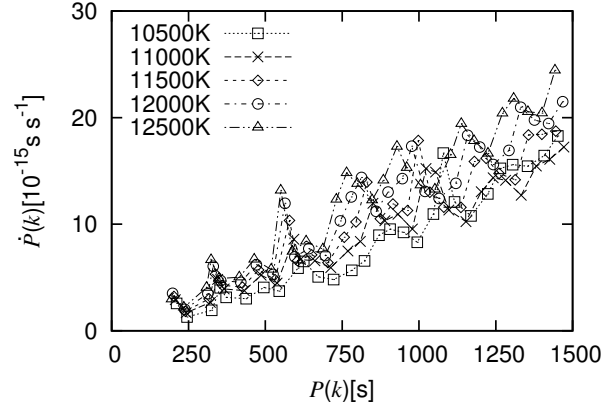
and down. In this subsection, we will discuss the effect of different values of M_* and T_eff on the rate of period change.

In Figure 8, we show a diagram of $\dot{P}(k)$ versus $P(k)$ with different M_* values. The model parameters are

$$\log(M_\mathrm{H}/M_*) = -4.0,$$

$$\log(M_\mathrm{He}/M_*) = -2.0,$$

M_* from $0.550\,M_\odot$ to $0.750\,M_\odot$ with steps of $0.050\,M_\odot$, and $T_\mathrm{eff} = 12\,200$ K and $11\,800$ K. We can see that the larger the total stellar mass of a DAV star, the smaller the rate of period change of its modes, especially for long-period modes. On one hand, a white dwarf with large stellar mass undergoes a long process of cooling down and therefore has a small cooling rate. A small cooling rate leads to a small rate of period change. On the other hand, a white dwarf with large stellar mass has a large gravitational acceleration and a small asymptotic period spacing according to Equation (2). The radial order k is from 1 to 29 for the model of $M_* = 0.550\,M_\odot$ and from 1 to 38 for the model of $M_* = 0.750\,M_\odot$ in the period range of 0–1500 s. Therefore, the asymptotic period spacing is small for the model of $M_* = 0.750\,M_\odot$. Both the long process of cooling down and the small value of asymptotic period spacing lead to obviously small rate of period change for long-period modes of large stellar mass DAV stars.

In Figure 9, we show a diagram of $\dot{P}(k)$ versus $P(k)$ with different T_eff values. The effective temperature is from $12\,500$ K to $10\,500$ K with steps of 500 K. The rate of period change with $T_\mathrm{eff} = 12\,500$ K is calculated from two models of $T_\mathrm{eff} = 12\,700$ K and $12\,300$ K, namely
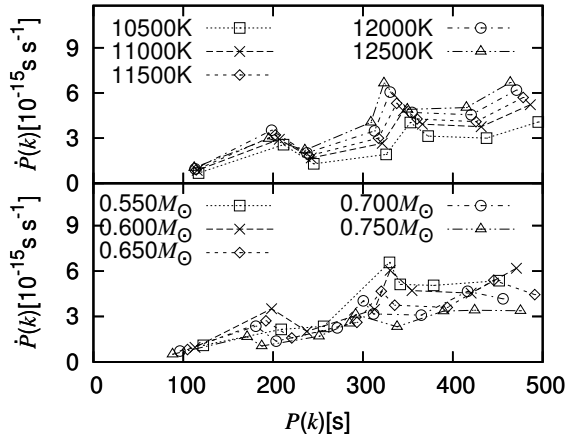
Fig. 10 An enlargement of Figs. 8 and 9 for short-period modes.

$\Delta T_{\mathrm{eff}} = 400\,\mathrm{K}$. We can see that the higher the effective temperature, the larger the rate of period change. This is because the hot DAV star cools faster. The radial order k is from 1 to 29 for the model of $T_{\mathrm{eff}} = 10\,500\,\mathrm{K}$ and from 1 to 31 for the model of $T_{\mathrm{eff}} = 12\,500\,\mathrm{K}$. Therefore, the change of asymptotic period spacing has a small effect on the rate of period change for models with different T_{eff} values. Different cooling rates for different DAV star models dominate the values of $\dot{P}(k)$.

For long-period modes, the effect of different values of M_* and T_{eff} is relatively obvious. If we observe a large $\dot{P}(k)$ for a long-period mode, the star may have a small M_* or a high T_{eff}. Short-period modes in Figures 8 and 9 are enlarged in Figure 10. In the upper panel in Figure 10, both the different T_{eff} values and different KEDs have an effect on the rate of period change. However, in the lower panel, different kinetic energy distributions dominate the distributions of $\dot{P}(k)$.

4 THE RATE OF PERIOD CHANGE IN G117–B15A AND R548

Based on the discussions above, the values of $\dot{P}(k)$ are determined by KED of $P(k)$, the stellar mass M_* and the effective temperature T_{eff}. In this section, we study the rate of period change in DAV stars G117–B15A and R548. Grids of DAV star models are evolved. The pre-grid parameters are shown in the last paragraph of Section 2. The eigen-frequencies are scanned out among the grids of DAV star models and are used to fit the observed modes of G117–B15A and R548. A pre-best-

Table 2 The observed modes from table 5 of Romero et al. (2012) and calculated modes from corresponding best-fitting models. The value of P_{obs} minus P_{cal} and the parameter χ are also displayed. For R548, a new mode of 217.83 s was identified by Giammichele et al. (2015).

Star	$P_{\mathrm{obs}}(l)$ [s]	$P_{\mathrm{cal}}(l,k)$ [s]	P_{obs}-P_{cal} [s]	χ [s]
G117–B15A	215.20(1)	213.86(1,1)	1.34	1.32
	270.46(1)	270.92(1,2)	–0.46	
	304.05(1)	305.85(1,3)	–1.80	
R548	187.28(1 or 2)	190.42(2,3)	–3.14	2.12
	212.95(1)	214.41(1,1)	–1.46	
	274.51(1)	272.48(1,2)	2.03	
	318.07(1 or 2)	317.97(1,3)	0.10	
	333.64(1 or 2)	331.13(1,4)	2.51	
R548	217.83(2)	218.82(2,4)	–0.99	1.97

fitting model is selected by,

$$\chi = \sqrt{\frac{\sum_1^{n_{\mathrm{obs}}}(P_{\mathrm{cal}} - P_{\mathrm{obs}})^2}{n_{\mathrm{obs}}}}. \quad (6)$$

In Equation (6), P_{cal} is the calculated modes, P_{obs} is the observed modes and n_{obs} is the number of observed modes. The model with minimal χ is selected as the pre-best-fitting one. Then, the grids of DAV star models will be made dense around the pre-best-fitting parameters. Next, a best-fitting model will be selected according to Equation (6). We will calculate the rate of period change of modes from the best-fitting model and compare them with the corresponding observed rate of period change obtained through the $O - C$ method.

4.1 Asteroseismological Study on DAV Stars G117–B15A and R548

The observed modes of G117–B15A and R548 are from table 5 of Romero et al. (2012). They are listed in Table 2, marked as $P_{\mathrm{obs}}(l)$, in this paper. We assume them to be $m = 0$ modes. The modes we calculated are all $m = 0$ modes. G117–B15A was identified as a DAV star by Richer & Ulrych (1974). The variability of G117–B15A was confirmed by McGraw & Robinson (1976) with three modes. Kepler et al. (1982) identified six modes, including the three modes, for G117–B15A. The three other modes can be explained by nonlinear pulsation effects (Brassard et al. 1993). The cancelation effect of neighboring parts leads to high l modes that are not easy to observe. Therefore, the three modes are basically assumed to be $l = 1$ modes. This assumption is consistent with previous work (Robinson et al. 1995; Bradley 1998; Benvenuto et al. 2002). Bradley (1998) and Benvenuto et al. (2002) fitted them by consecutive $l = 1$ modes with

the 215 s mode being either a $k = 1$ or a $k = 2$ mode. We also assume them to be $l = 1$ modes. R548 was identified as a harmonically variable white dwarf by Lasker & Hesser (1970, 1971). Stover et al. (1980) identified the double modes of 213 s and 274 s. Kepler et al. (1995) detected three other small-amplitude modes near 187, 320 and 333 s. We assume the two doublets to be $l = 1$ modes and the three singlets to be $l = 1$ or 2 modes, as shown in Table 2.

Fitting the observed modes in the second column of Table 2, a pre-best-fitting model is selected for each star. The pre-best-fitting model fitting G117–B15A is model1 in Table 3 and the pre-best-fitting model fitting R548 is model7 in Table 3. Then, the grid models are made dense. For G117–B15A, $\log(M_{\mathrm{H}}/M_*)$ is from –7.0 to -9.0 with steps of 0.5, $\log(M_{\mathrm{He}}/M_*)$ is from –2.0 to –4.0 with steps of 0.5, M_* is from $0.640\,M_\odot$ to $0.680\,M_\odot$ with steps of $0.005\,M_\odot$, and T_{eff} is from $11\,600\,\mathrm{K}$ to $12\,200$ K with steps of 50 K. For R548, $\log(M_{\mathrm{H}}/M_*)$ is from –7.0 to –9.0 with steps of 0.5, $\log(M_{\mathrm{He}}/M_*)$ is from –2.0 to –4.0 with steps of 0.5, M_* is from $0.630\,M_\odot$ to $0.670\,M_\odot$ with steps of $0.005\,M_\odot$, and T_{eff} is from $12\,300\,\mathrm{K}$ to $12\,800\,\mathrm{K}$ with steps of 50 K. Fitting G117–B15A and R548, the parameters of ten models with the smallest χs are shown in Table 3. The values of χ are only slightly different. We do not suggest that model1 must have a clear advantage over model2. In mathematical fitting, the value of χ for model1 is slightly smaller than that for other models. Therefore, model1 is marked as the best-fitting model.

Fitting G117–B15A, the ten models with the smallest χs have parameters of $\log(M_{\mathrm{H}}/M_*) = -8.0$, $\log(M_{\mathrm{He}}/M_*) = -3.0$, $M_* = 0.655 - 0.665\ M_\odot$, $T_{\mathrm{eff}} = 11\,700 - 12\,000\,\mathrm{K}$ and $\log g = 8.1825 - 8.1941$. Fitting R548, the ten models with the smallest χs have parameters of $\log(M_{\mathrm{H}}/M_*) = -8.0$, $\log(M_{\mathrm{He}}/M_*) = -3.5$, $M_* = 0.645 - 0.650\ M_\odot$, $T_{\mathrm{eff}} = 12\,450 - 12\,800\,\mathrm{K}$ and $\log g = 8.1712 - 8.1800$. According to the new work of Giannins et al. (2011) on the DAV instability strip, model10 with $T_{\mathrm{eff}} = 12\,800\,\mathrm{K}$ and $\log g = 8.1712$ is within the DAV instability strip.

The color residual diagrams of fittings for G117–B15A and R548 are shown in Figures 11 and 12 respectively. The abscissa is the stellar mass M_* and the ordinate is the effective temperature T_{eff}. The parameter χ is represented by color.

The values of H and He are the same as the models in Table 3. The calculated periods for the two best-fitting models are shown in Table 2. For G117–B15A, the three observed modes are fitted by $l = 1$ modes. The radial
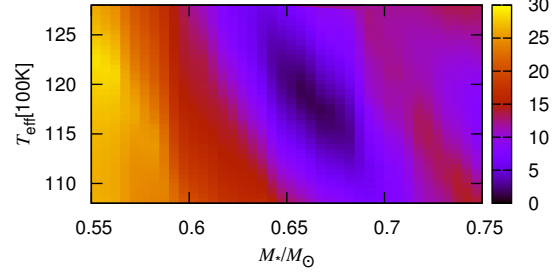

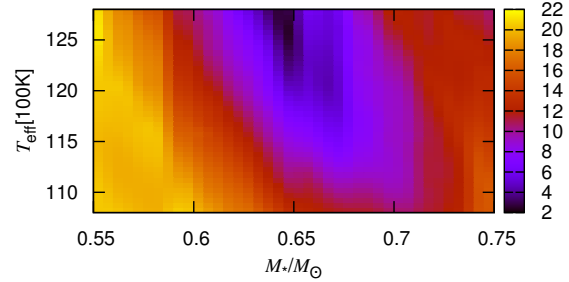**Fig. 11** Color residual diagram for fitting G117–B15A. The color scale refers to the χ value.

Fig. 12 Color residual diagram for fitting R548. The color scale refers to the χ value.

order k is 1, 2 and 3 respectively. The absolute value of P_{obs} minus P_{cal} is less than 2.00 s and χ is 1.32 s. For R548, the maximal absolute value of P_{obs} minus P_{cal} is 3.14 s and the parameter χ is 2.12 s. In addition, a possible single mode of 217.83 s with S/N = 3.9 is identified by Giammichele et al. (2015) for R548. The mode of 213 s is assumed to be an $l = 1$ mode. The new mode seems to be an $l = 2$ mode. We assume $m = 0$ for the mode. The corresponding best-fitting model just has a mode of 218.82 s ($l = 2$, $k = 4$). The absolute value of P_{obs} minus P_{cal} is 0.99 s for the new mode, which is relatively small. Calculating the six modes for R548 together, the best-fitting model has the value of $\chi = 1.97$ s. The six modes are fitted by four $l = 1$ modes and two $l = 2$ modes, as shown in Table 2.

4.2 Comparing the Stellar Parameters to Previous Spectroscopic Results and Asteroseismological Results

In Table 4, we show the previous spectroscopic results. Studying the optical spectra and ultraviolet spectra of DAV stars, Bergeron et al. (1995) suggested that the best value of the mixing length parameter is ML2/$\alpha = 0.6$. In our model evolutions by WDEC, the mixing length pa-

Table 3 The Parameters of Ten Fitting Models with Smallest χs Fitting G117–B15A and R548

	$\log(M_H/M_*)$	$\log(M_{He}/M_*)$	T_{eff} [K]	M_* [$M_\odot$]	$\log g$	χ [s]
ID(G117–B15A)						
model1	−8.0	−3.0	11 900	0.660	8.1912	1.32
model2	−8.0	−3.0	11 950	0.660	8.1911	1.33
model3	−8.0	−3.0	11 750	0.665	8.1940	1.44
model4	−8.0	−3.0	11 850	0.660	8.1913	1.48
model5	−8.0	−3.0	12 000	0.660	8.1910	1.50
model6	−8.0	−3.0	11 800	0.665	8.1939	1.51
model7	−8.0	−3.0	11 700	0.665	8.1941	1.56
model8	−8.0	−3.0	11 850	0.665	8.1938	1.72
model9	−8.0	−3.0	12 000	0.655	8.1825	1.74
model10	−8.0	−3.0	11 800	0.660	8.1914	1.75
ID(R548)						
model1	−8.0	−3.5	12 650	0.645	8.1714	2.12
model2	−8.0	−3.5	12 600	0.645	8.1715	2.16
model3	−8.0	−3.5	12 700	0.645	8.1713	2.19
model4	−8.0	−3.5	12 550	0.645	8.1716	2.29
model5	−8.0	−3.5	12 750	0.645	8.1712	2.35
model6	−8.0	−3.5	12 500	0.645	8.1717	2.50
model7	−8.0	−3.5	12 500	0.650	8.1799	2.51
model8	−8.0	−3.5	12 550	0.650	8.1798	2.54
model9	−8.0	−3.5	12 450	0.650	8.1800	2.57
model10	−8.0	−3.5	12 800	0.645	8.1712	2.58

rameter is also set as ML2/α = 0.6. Bergeron et al. (1995) reported the spectral result of T_{eff} and $\log g$ for 22 DAV stars, including G117–B15A and R548, as shown in Table 4. Based largely on the last published version of the McCook & Sion (1999) catalog, Gianninas et al. (2011) conducted a spectroscopic study on over 1100 bright DA white dwarfs (optical spectra) with improved models. The detailed spectral parameters are shown in table 5 of Gianninas et al. (2011). Their results for G117–B15A and R548 are selected in Table 4. With ML2/α = 0.6, Koester & Holberg (2001) studied 11 DAV stars based on their ultraviolet spectra from IUE or HST. Their results for G117–B15A (WD0921+354) and R548 (WD0133-116) are selected, as shown in Table 4. Spectral work depends strongly on the theoretical treatment of convection. The convective efficiency of ML2/α = 0.7 is more appropriate for the spectroscopic work of Giammichele et al. (2015) on DAV stars GD165 and R548. Tremblay et al. (2013) described the first grid of mean three-dimensional (3D) spectra for DA white dwarfs based on 3D model atmospheres. Taking the 1D/3D corrections of Tremblay et al. (2013) into account, Giammichele et al. (2015) obtained new spectral results for R548.

For G117–B15A, the values of T_{eff} = 11 700 − 12 000 K in Table 3 are consistent with those of B1995 and K2001, but slightly smaller than those of G2011 in Table 4. The values of $\log g$ = 8.1825−8.1941 in Table 3 are basically consistent with those of G2011 but slightly

Table 4 The previous spectroscopic results of Bergeron et al. (1995) (B1995 for short), Gianninas et al. (2011) (G2011 for short), Koester & Holberg (2001) (K2001 for short) and Giammichele et al. (2015) (G2015 for short).

Reference	T_{eff} [K]	$\log g$
G117–B15A		
B1995	11 620±200	7.97±0.05
G2011	12 600±193	8.14±0.05
K2001	12 010±180	7.94±0.17
R548		
B1995	11 990±200	7.97±0.05
G2011	12 480±190	8.05±0.05
K2001	11 865±170	7.89±0.17
G2015	12 204±190	8.012±0.048

larger than those of B1995 and K2001 in Table 4. For R548, the values of T_{eff} = 12 450 − 12 800 K in Table 3 are consistent with those of G2011 but slightly larger than those of B1995, K2001 and G2015 in Table 4. The values of $\log g$ = 8.1712 − 8.1800 in Table 3 are slightly larger than those of B1995, G2011, K2001 and G2015 in Table 4. Overall, the gravitational accelerations are slightly larger for our models. The gravitational acceleration is calculated by $\frac{GM}{R^2}$. It may be associated with the stellar radius, which will be studied in future work.

In Table 5, we show the asteroseismological results of Castanheira & Kepler (2008, 2009), Bischoff-Kim et al. (2008a), Romero et al. (2012) and Giammichele et al. (2016). Castanheira & Kepler (2008, 2009) evolved

Table 5 The asteroseismological results of Castanheira & Kepler (2008, 2009) (C2008 and C2009 for short), Bischoff-Kim et al. (2008a) (B2008a for short), Romero et al. (2012) (R2012 for short) and Giammichele et al. (2016) (G2016 for short).

Reference	$\log(M_H/M_*)$	$\log(M_{He}/M_*)$	T_{eff} [K]	M_* [$M_\odot$]	k	χ [s]
G117–B15A						
$l=1$						
C2008	−7.0	−2.0	12 000	0.615	1,2,3	2.85
	−5.0	−2.5	11 500	0.750	2,3,4	3.84
	−7.5	−3.0	12 600	0.710	1,2,3	2.94
	−8.5	−3.5	11 500	0.850	1,2,4	0.74
B2008a	−6.2	−2.4	11 400–12 200	0.650–0.680	2,3,4	
	(−8.0)–(−7.4)	−2.4	11 800–12 600	0.600–0.640	1,2,3	
R2012	(−6.2)–(−5.7)	−1.6	11 985±200	0.593±0.007	2,3,4	2.14
This paper	−8.0	−3.0	11 900	0.660	1,2,3	1.32
R548						
$l=1$ or 2						
C2009	−4.5	−2.0	12 100	0.635		2.64
	−5.5	−2.5	11 000	0.790		3.91
B2008a	(−7.2)–(−7.7)	−2.4	11 700–12 600	0.600–0.650		
R2012	−6.0	−1.6	11 627±390	0.609±0.012		3.42
G2016	−7.45±0.12	−2.92±0.10	12 281±125	0.65±0.02		0.59
This paper	−8.0	−3.5	12 650	0.645		2.12(1.97)

grids of DAV star models by WDEC with homogeneous C/O core compositions and performed an asteroseismological study on over 80 DAV stars, including G117–B15A and R548. They obtained four 'best-fitting' models fitting G117–B15A, and two 'best-fitting' models fitting R548. Bischoff-Kim et al. (2008a) evolved grids of DAV star models by WDEC based on chemical composition profiles of a fiducial model and models with a sharper C/He transition zone, as shown in figure 2 of Bischoff-Kim et al. (2008a). They conducted an asteroseismological study on G117–B15A and R548. Their best-fitting models with 'thick' H and thin H for G117–B15A, and thin H for R548 are displayed in Table 5. Romero et al. (2012) made fully evolutionary DA white dwarf models characterized by detailed chemical profiles by the LPCODE evolutionary code. Based on those DAV star models, they performed an asteroseismological study on 44 bright DAV stars, including G117–B15A and R548. In addition, Giammichele et al. (2016) did an asteroseismological study on GD165 and R548 based on parameterized static models. Their best-fitting model is shown in Table 5. According to those best-fitting models in Table 5, the values of corresponding χ are calculated. All the values are smaller than 4.00 s. We notice that the best-fitting models depend on the stellar evolution code, such as the input core composition profiles.

For G117–B15A, the three modes are fitted by the best-fitting model (model1 in Table 3) with $k = 1, 2, 3$ mode ($l = 1$) respectively. They are fitted by the model of Romero et al. (2012) with $k = 2, 3, 4$ mode ($l = 1$) respectively. That is why we obtain a thin H mass model and they have a relatively thick H mass model. The discussion about thin H mass or thick H mass had been reported in detail by Bradley (1998) and Benvenuto et al. (2002). Bischoff-Kim et al. (2008a) obtained a group of relatively 'thick' H mass models ($k = 1, 2, 3$) and a group of thin H mass models ($k = 2, 3, 4$). The three observed modes are fitted by Castanheira & Kepler (2008) with $k = 1, 2, 3$ modes for thin H models, except for one with a large mass ($M_* = 0.850\,M_\odot$), and with $k = 2, 3, 4$ modes ($l = 1$) for thick H models. For the model of $M_* = 0.850\,M_\odot$, the three modes are fitted by $k = 1, 2, 4$ modes, as shown in the sixth column in Table 5.

For R548, the five modes are fitted by four $l = 1$ modes and one $l = 2$ mode for the best-fitting model (model1 in Table 3), as shown in Table 2. The mode of 187 s is fitted by an $l = 2$ and $k = 3$ mode. The other modes are fitted by $l = 1$ and $k = 1, 2, 3, 4$ modes respectively. The best-fitting model fitting R548 is similar to the best-fitting model fitting G117–B15A. The two best-fitting models are thin H models with $\log(M_H/M_*) = −8.0$, as shown in Table 3. Castanheira & Kepler (2009) and Romero et al. (2012) obtained relatively thick H mass models fitting R548. For the first model of Castanheira & Kepler (2009), the modes of 187 s and 333 s are fitted by $l = 2$ and $k = 3, 9$ modes. The other three modes are fitted by $l = 1$ and $k = 1, 2, 3$

modes. For the second model of Castanheira & Kepler (2009), the mode of 187 s is fitted by an $l = 2$ and $k = 3$ mode while the other four modes are fitted by $l = 1$ and $k = 2, 3, 4, 5$ modes. For the best-fitting model of Romero et al. (2012), the modes of 318 s and 333 s are fitted by $l = 2$, $k = 8, 9$ modes. The other three modes are fitted by $l = 1$ and $k = 1, 2, 3$ modes. For the models of Bischoff-Kim et al. (2008a), the modes of 187 s and 334 s are fitted by $l = 2$ and $k = 4, 8$ modes. The other three modes are fitted by $l = 1$ and $k = 1, 2, 4$ modes. The mode identifications of our best-fitting model are not consistent with their results.

Giammichele et al. (2016) did an asteroseismological study on R548 based on parameterized static models from the optimization package LUCY (Charpinet et al. 2015). They obtained a best-fitting model with thin H mass. Their best-fitting model parameters are

$$\log(M_H/M_*) = -7.45 \pm 0.12,$$

$$\log(M_{He}/M_*) = -2.92 \pm 0.10,$$

$$M_* = 0.65 \pm 0.02 \, M_\odot,$$

$T_{eff} = 12\,281 \pm 125$ K and $\log g = 8.108 \pm 0.025$. Their asteroseismological study on R548 is basically consistent with their spectroscopic work with $T_{eff} = 12\,204 \pm 190$ K and $\log g = 8.012 \pm 0.048$. For their best-fitting model, the modes of 187 s and 217 s are fitted by $l = 2$ and $k = 3, 4$ modes. The other four modes are fitted by $l = 1$ and $k = 1, 2, 3, 4$ modes. The mode identifications of our best-fitting model are the same with those of the best-fitting model of Giammichele et al. (2016). In addition, the values of H, He, T_{eff} and M_* for our best-fitting model are consistent with or close to those of the best-fitting model of Giammichele et al. (2016), as shown in Table 5.

4.3 Comparing the Rates of Period Change to the Observed Values Obtained Through the $O - C$ Method

Based on the observations of G117–B15A from 1974 to 2010, Kepler (2012) reported the rate of period change for 215 s as $(4.89 \pm 0.53) \times 10^{-15}$ s s^{-1}. The proper motion correction is $(-0.7 \pm 0.2) \times 10^{-15}$ s s^{-1}. Namely, the value of $\dot{P}_{obs}$ is $(4.19 \pm 0.73) \times 10^{-15}$ s s^{-1} for the 215 s mode of G117–B15A, as shown in Table 6. For our best-fitting model, the mode of 213.86 s ($l = 1, k = 1$) is used to fit the 215 s mode. We calculate the rate of period change for the mode of $l = 1$ and $k = 1$. The value of $\dot{P}_{cal}$ is just 4.19×10^{-15} s s^{-1}, which is exactly consistent with the observed value. For the mode of

Table 6 Comparing the calculated values of $\dot{P}$ of the two best-fitting models in Table 3 to the observed values of that obtained through the $O - C$ method for G117–B15A and R548.

Star	P_{obs} [s]	$\dot{P}_{obs}$ [10^{-15} s s^{-1}]	$P_{cal}(l,k)$ [s]	$\dot{P}_{cal}$ [10^{-15} s s^{-1}]
G117–B15A	215.20	4.19±0.73	213.86(1,1)	4.19
	270.46		270.92(1,2)	2.40
	304.05		305.85(1,3)	3.96
R548	187.28		190.42(2,3)	2.25
	212.95	3.3±1.1	214.41(1,1)	4.21
	217.83		218.82(2,4)	3.75
	274.51		272.48(1,2)	2.15
	318.07		317.97(1,3)	5.39
	333.64		331.13(1,4)	4.02

213.86 s ($l = 1, k = 1$), 96.44% of the kinetic energy is distributed in the He layer.

The DAV star R548 has been observed from 1970 November to 2012 January. Using 41 years of time-series photometry, Mukadam et al. (2013) calculated the rate of period change for the 213 s mode. Taking the correction of proper motion into account, Mukadam et al. (2013) obtained $\dot{P}_{obs} = (3.3 \pm 1.1) \times 10^{-15}$ s s^{-1} for the 213 s mode. For our best-fitting model, the mode of 214.41 s ($l = 1, k = 1$) is used to fit the 213 s mode of R548. We calculate the rate of period change for the mode of $l = 1$ and $k = 1$. The value of $\dot{P}_{cal}$ is 4.21×10^{-15} s s^{-1}, which is consistent with the observed value. Fitting the mode of 213 s, 95.61% of the kinetic energy is distributed in the He layer for the mode of 214.41 s ($l = 1, k = 1$). Giammichele et al. (2016) obtained the calculated value of $(2.87–2.91) \times 10^{-15}$ s s^{-1} for the corresponding mode. It is consistent with the observed value. If the value of $\dot{P}_{cal}$ is smaller than the value of $\dot{P}_{obs}$, the results can be used to constrain the axion mass (Bischoff-Kim et al. 2008b; Córsico et al. 2012a,b, 2016; Mukadam et al. 2013). However, the two modes of our best-fitting models fitting the 215 s mode of G117–B15A and the 213 s mode of R548 are trapped or partly trapped in the He layer. They have relatively large rates of period change. The values are consistent with observed values.

5 DISCUSSION AND CONCLUSIONS

In this paper, we introduce a method of evolving DAV stars. Groups of MS stars are evolved to be WD stars by a module named 'make_co_wd' from MESA (version 6208). The core compositions are taken out and added into WDEC. With historically viable core compositions, grids of DAV star models are evolved by WDEC, taking the element diffusion into account (Thoul et al. 1994; Su

et al. 2014). Those DAV star models are used to study the rate of period change in DAV stars. Then, we do an asteroseismological study on DAV stars G117–B15A and R548 based on the grids of DAV star models. Finally, we compare the calculated rates of period change with the observed values through the $O - C$ method.

Studying the rate of period change in DAV stars, we try to discuss the effect of different values of H atmosphere mass, He layer mass, stellar mass M_* and effective temperature $T_{\rm eff}$. Different thicknesses of H atmosphere and He layer will affect the rate of period change by the mode trapping effect. Modes trapped or partly trapped in the C/O core or He layer have a relatively large rate of period change, but modes trapped or partly trapped in the H atmosphere have a relatively small rate of period change. This is due to the fast cooling process of the C/O core and He layer. The cooling process dominates the rate of period change in DAV stars. The results are consistent with previous work (Bradley & Winget 1991; Bradley et al. 1992). The rate of period change is sensitive to the stellar mass and the effective temperature. A large M_* DAV star has a long process of cooling down and then a small rate of period change (Bradley & Winget 1991; Bradley 1996). A high $T_{\rm eff}$ DAV star has a fast time for cooling down and then a large rate of period change. The effect of different values of M_* and $T_{\rm eff}$ is obvious for long-period modes.

Based on the observed modes of G117–B15A and R548 from Romero et al. (2012), we evolve grids of DAV star models and conduct an asteroseismological study on the two DAV stars. A best-fitting model is selected for each star by selecting a minimal value of χ. The two DAV stars have short-period modes observed, as shown in Table 2, and therefore they should have hot effective temperatures (Clemens 1993; Mukadam et al. 2006). The corresponding two best-fitting models are really hot DAV star models, with $T_{\rm eff} = 11\,900\,{\rm K}$ for G117–B1A and $T_{\rm eff} = 12\,650\,{\rm K}$ for R548. For the fitting results, the maximal absolute value of observed mode minus calculated mode is 3.14 s. The value of χ is respectively 1.32 s fitting G117–B15A and 2.12 s fitting R548. In addition, the new observed mode of 217.83 s (Giammichele et al. 2015) for R548 can also be fitted by a mode of 218.82 s ($l = 2, k = 4$) for the best-fitting model.

The DAV stars G117–B15A and R548 are observationally similar. The best-fitting model fitting R548 is similar to the best-fitting model fitting G117–B15A. The calculated rate of period change for the mode of 213 s for R548 is also similar to that for the mode of 215 s for G117–B15A. Based on the two best-fitting models,

the mode identifications (l, k) of the observed modes for G117–B15A and R548 are consistent with previous work for G117–B15A (thin H model of Bradley 1998; Benvenuto et al. 2002; Castanheira & Kepler 2008; Bischoff-Kim et al. 2008a) and R548 (Giammichele et al. 2016). In addition, fitting G117–B15A, the calculated rate of period change is exactly consistent with the corresponding observed one through $O - C$. Fitting R548, the calculated rate of period change is consistent with the corresponding observed one. Basically, both the observed modes and observed rates of period change obtained through the $O - C$ method can be fitted. The results greatly increase our confidence in the asteroseismological study on DAV stars. The results indicate that the method of evolving DAV stars (MESA(core)+WDEC(diffusion)) is feasible.

References

Benvenuto, O. G., Córsico, A. H., Althaus, L. G., & Serenelli, A. M. 2002, MNRAS, 332, 399

Bergeron, P., Wesemael, F., Lamontagne, R., et al. 1995, ApJ, 449, 258

Bischoff-Kim, A., & Metcalfe, T. S. 2011, MNRAS, 414, 404

Bischoff-Kim, A., Montgomery, M. H., & Winget, D. E. 2008a, ApJ, 675, 1505

Bischoff-Kim, A., Montgomery, M. H., & Winget, D. E. 2008b, ApJ, 675, 1512

Bradley, P. A., & Winget, D. E. 1991, ApJS, 75, 463

Bradley, P. A., Winget, D. E., & Wood, M. A. 1992, ApJ, 391, L33

Bradley, P. A. 1996, ApJ, 468, 350

Bradley, P. A. 1998, ApJS, 116, 307

Bradley, P. A. 2001, ApJ, 552, 326

Brassard, P., Fontaine, G., Wesemael, F., & Hansen, C. J. 1992, ApJS, 80, 369

Brassard, P., Fontaine, G., Wesemael, F., & Talon, A. 1993, in NATO Advanced Science Institutes (ASI) Series C, 403, ed. M. A. Barstow, 485

Castanheira, B. G., & Kepler, S. O. 2008, MNRAS, 385, 430

Castanheira, B. G., & Kepler, S. O. 2009, MNRAS, 396, 1709

Castanheira, B. G., Kepler, S. O., Kleinman, S. J., Nitta, A., & Fraga, L. 2010, MNRAS, 405, 2561

Charpinet, S., Giammichele, N., Brassard, P., Van Grootel, V., & Fontaine, G. 2015, in Astronomical Society of the Pacific Conference Series, 493, 19th European Workshop on White Dwarfs, eds. P. Dufour, P. Bergeron, & G. Fontaine, 151

Chen, Y.-H. 2016a, RAA (Research in Astronomy and Astrophysics), 16, 120

Chen, Y. H. 2016b, MNRAS, 458, 1190

Chen, Y. H., & Li, Y. 2014a, MNRAS, 443, 3477

Chen, Y. H., & Li, Y. 2014b, MNRAS, 437, 3183

Christensen-Dalsgaard, J. 2008, Ap&SS, 316, 113

Clemens, J. C. 1993, Baltic Astronomy, 2, 407

Córsico, A. H., Althaus, L. G., Miller Bertolami, M. M., et al. 2012a, MNRAS, 424, 2792

Córsico, A. H., Althaus, L. G., Romero, A. D., et al. 2012b, J. Cosmol. Astropart. Phys., 12, 010

Córsico, A. H., Romero, A. D., Althaus, L. G., et al. 2016, J. Cosmol. Astropart. Phys., 7, 036

Costa, J. E. S., & Kepler, S. O. 2008, A&A, 489, 1225

Dalessio, J., Sullivan, D. J., Provencal, J. L., et al. 2013, ApJ, 765, 5

Fu, J.-N., Vauclair, G., & Dolez, N. 2002, in Astronomical Society of the Pacific Conference Series, 256, Observational Aspects of Pulsating B- and A Stars, eds. C. Sterken & D. W. Kurtz, 51

Giammichele, N., Fontaine, G., Bergeron, P., et al. 2015, ApJ, 815, 56

Giammichele, N., Fontaine, G., Brassard, P., & Charpinet, S. 2016, ApJS, 223, 10

Gianninas, A., Bergeron, P., & Fontaine, G. 2005, ApJ, 631, 1100

Gianninas, A., Bergeron, P., & Ruiz, M. T. 2011, ApJ, 743, 138

Itoh, N., Mitake, S., Iyetomi, H., & Ichimaru, S. 1983, ApJ, 273, 774

Itoh, N., Kohyama, Y., Matsumoto, N., & Seki, M. 1984, ApJ, 285, 758

Kepler, S. O., Nather, R. E., McGraw, J. T., & Robinson, E. L. 1982, ApJ, 254, 676

Kepler, S. O., Giovannini, O., Costa, A. F. M., et al. 1995, Baltic Astronomy, 4, 238

Kepler, S. O., Mukadam, A., Winget, D. E., et al. 2000, ApJ, 534, L185

Kepler, S. O., Costa, J. E. S., Mukadam, A., et al. 2005a, in Astronomical Society of the Pacific Conference Series, 334, 14th European Workshop on White Dwarfs, eds. D. Koester & S. Moehler, 501

Kepler, S. O., Costa, J. E. S., Castanheira, B. G., et al. 2005b, ApJ, 634, 1311

Kepler, S. O. 2012, in Astronomical Society of the Pacific Conference Series, 462, Progress in Solar/Stellar Physics with Helio- and Asteroseismology, eds. H. Shibahashi, M. Takata, & A. E. Lynas-Gray, 322

Koester, D., & Holberg, J. B. 2001, in Astronomical Society of the Pacific Conference Series, 226, 12th European Workshop on White Dwarfs, eds. J. L. Provencal, H. L. Shipman, J. MacDonald, & S. Goodchild, 299

Kutter, G. S., & Savedoff, M. P. 1969, ApJ, 156, 1021

Lamb, Jr., D. Q. 1974, Evolution of Pure Carbon-12 White Dwarfs., PhD Thesis, The University of Rochester

Lamb, D. Q., & van Horn, H. M. 1975, ApJ, 200, 306

Lasker, B. M., & Hesser, J. E. 1970, IAU Circ., 2291

Lasker, B. M., & Hesser, J. E. 1971, ApJ, 163, L89

Li, Y. 1992a, A&A, 257, 145

Li, Y. 1992b, A&A, 257, 133

McCook, G. P., & Sion, E. M. 1999, ApJS, 121, 1

McGraw, J. T., & Robinson, E. L. 1976, ApJ, 205, L155

Montgomery, M. H., Klumpe, E. W., Winget, D. E., & Wood, M. A. 1999, ApJ, 525, 482

Mukadam, A. S., Montgomery, M. H., Winget, D. E., Kepler, S. O., & Clemens, J. C. 2006, ApJ, 640, 956

Mukadam, A. S., Bischoff-Kim, A., Fraser, O., et al. 2013, ApJ, 771, 17

Paxton, B., Bildsten, L., Dotter, A., et al. 2011, ApJS, 192, 3

Paxton, B., Cantiello, M., Arras, P., et al. 2013, ApJS, 208, 4

Richer, H. B., & Ulrych, T. J. 1974, ApJ, 192, 719

Robinson, E. L., Mailloux, T. M., Zhang, E., et al. 1995, ApJ, 438, 908

Romero, A. D., Córsico, A. H., Althaus, L. G., et al. 2012, MNRAS, 420, 1462

Saumon, D., Chabrier, G., & van Horn, H. M. 1995, ApJS, 99, 713

Stover, R. J., Nather, R. E., Robinson, E. L., Hesser, J. E., & Lasker, B. M. 1980, ApJ, 240, 865

Su, J., Li, Y., Fu, J.-N., & Li, C. 2014, MNRAS, 437, 2566

Tassoul, M. 1980, ApJS, 43, 469

Thoul, A. A., Bahcall, J. N., & Loeb, A. 1994, ApJ, 421, 828

Tremblay, P.-E., Ludwig, H.-G., Steffen, M., & Freytag, B. 2013, A&A, 559, A104

Winget, D. E., Hansen, C. J., & van Horn, H. M. 1983, Nature, 303, 781

Winget, D. E., & Kepler, S. O. 2008, ARA&A, 46, 157

Winget, D. E., van Horn, H. M., & Hansen, C. J. 1981, ApJ, 245, L33

Wood, M. A. 1990, Astero-archaeology: Reading the Galactic History Recorded in the White Dwarf Stars, PhD Thesis, Univ. of Texas at Austin